A study on the stability of O_2 on oxometalloporphyrins by the first principles calculations

Yoshiyuki Kubota
Department of Precision Science and Technology and Applied Physics, Osaka University, Suita, Osaka 565-0871, Japan and Power Engineering Research & Development Center, Research & Development Department, Kansai Electric Power Co., Inc., Amagasaki, Hyogo 661-0974, Japan

Mary Clare Sison Escaño, Eben Sy Dy, Hiroshi Nakanishi, and Hideaki Kasai
Department of Precision Science and Technology and Applied Physics, Osaka University, Suita, Osaka 565-0871, Japan

(Received 1 September 2006; accepted 29 March 2007; published online 15 May 2007)

The authors investigated the interaction of oxometalloporphyrins (MO(por))—specifically, MoO(por), WO(por), TiO(por), VO(por), and CrO(por)—with O_2 by using first principles calculations. MoO(por) and WO(por) undergo reactions with O_2; on the other hand, TiO(por), VO(por), and CrO(por) do not. Next, they compared the interaction of MoO(por) and WO(por) with O_2. Activation barriers for the reactions of MoO(por) and WO(por) with a side-on O_2 are small. For MoO(por)(O_2), the activation barrier for the reverse reaction that liberates O_2 is also small; however, that for WO(por)(O_2) is large. The experimental results that photoirradiation with visible light or heating of Mo ^{VI}O(tmp)(O_2) regenerates Mo ^{VI}O(tmp) by liberating O_2 while W ^{VI}O(tmp)(O_2) does not [J. Tachibana, T. Imamura, and Y. Sasaki, Bull. Chem. Soc. Jpn. **71**, 363 (1998)] are explained by the difference in activation barriers of the reverse reactions. This means that bonds formed between the W atom and O_2 are stronger than those between the Mo atom and O_2. The bond strengths can be explained by differences in the energy levels between the highest occupied molecular orbital of MoO(por) and WO(por), which are mainly formed from the *a* orbitals of the central metal atom and π^* orbitals of O_2. © *2007 American Institute of Physics*.
[DOI: 10.1063/1.2733645]

I. INTRODUCTION

In recent years, though it is more and more important to reduce global environment load, there is hardly any sign that the emission of greenhouse gases is decreasing. One of the methods to overcome this may be to replace existing fossil fuels used in thermal power generators, gasoline engines, or diesel engines with hydrogen gas used in fuel cells. There are many studies on hydrogen production and fuel cells. Particularly, we are focusing on polymer electrolyte fuel cells (PEFCs) which will greatly contribute to the reduction of greenhouse gases and can be used not only for stationary power generation of residences but also as mobile power sources of vehicles. As far as the fuel cell is concerned, the biggest problem is high cost when compared to other cogeneration systems. One of the reasons is the price of platinum—the rare metal used in both the anode and cathode of fuel cells. The key to successful commercial use of fuel cells is to discover how the amount of platinum used can be reduced or how cheap substances can replace platinum. Our laboratory has been studying various alternative catalyst systems for this purpose.[1–4]

In this paper, we consider using metalloporphyrin as a catalyst for electrodes. Metalloporphyrins such as dimetal bisporphyrins is experimentally observed to catalyze the four-electron reduction of O_2 to H_2O efficiently,[5–8] though they are difficult to synthesize because of the reaction processes involved. In the case of a monometal porphyrin, the selective two-electron reduction of O_2 to H_2O_2 occurs, but H_2O_2 decomposes polymer electrolytes.[9] It is known that dimetal bisporphyrins react with O_2 to produce the μ-peroxospecies, which have longer O–O bond length than that of gaseous O_2.[7] It is thought that the path of oxygen reduction (two electron versus four electron) is caused by differences in O–O bond length. We think that longer O–O bond lengths in dimetal bisporphyrins results in weakening of the O–O bond, favoring the four-electron reduction of O_2 to H_2O.

It is known that Mo ^{IV}O(tmp) undergoes a reaction with O_2 to form Mo ^{VI}O(tmp)(O_2) at room temperature[10,11] in the solid state. X-ray crystallography clarifies that the O_2 adsorbed in Mo ^{VI}O(tmp) takes a side-on configuration, as shown in Fig. 1(b), and the O–O bond length of the adsorbed O_2 is longer than that of gaseous O_2.[12] On the other hand, O_2 adsorbed in metalloporphyrins (without the oxogroup) ordinarily takes an end-on configuration, and their O–O bond hardly increases in length.[1,13,14]

We think that an increase in the O–O bond length of Mo ^{VI}O(tmp)(O_2) weakens the O–O bond and, thus, may lead to O_2 reduction pathway to H_2O formation as in the case of dimetal bisporphyrins.

In this paper, we investigate the MoO(por), WO(por), CrO(por), TiO(por), and VO(por). The stabilities and con-

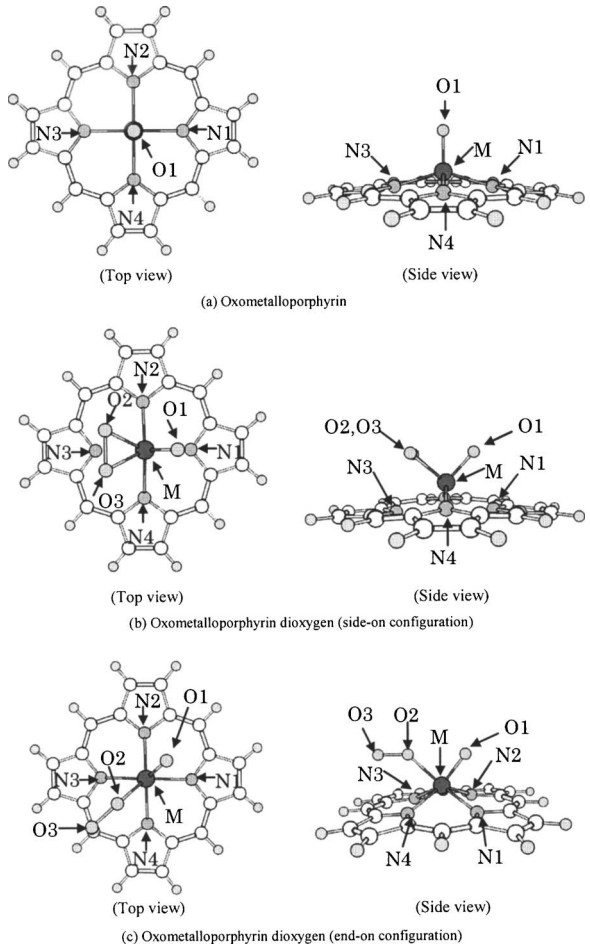

FIG. 1. The structures of oxometalloporphyrin (a) and two kinds of dioxygen complexes; (b) side-on configuration and (c) end-on configuration. M refers to the metal atom in the center of the porphyrin ring, and N1, N2, N3, and N4 are the nitrogen atoms, and O1, O2, and O3 are the oxygen atoms. The white spheres are carbon atoms, and the other small spheres are hydrogen atoms. The optimized structures for both the Mo complex and the W complex with side-on O_2 result in configurations such that N1 is eclipsed by O1, and N3 is eclipsed by the bond between O2 and O3, as shown in the top view of (b). On the other hand, those complexes with end-on O_2 configurations have O1 located between N1 and N2, and a carbon atom eclipsed by O3, as shown in the top view of (c).

figurations of these oxometalloporphyrins and oxometalloporphyrin dioxygens are calculated by first principles molecular dynamics. We clarify how the oxometalloporphyrins undergo a reaction with O_2 with respect to the molecular orbitals.

II. COMPUTATIONAL METHODS

The calculations were performed using the first principles simulation code Vienna *ab initio* simulation package (VASP) developed at the Institut für Theoretische Physik of the Technische Universität Wien.[15–18] Vanderbilt ultrasoft pseudopotentials[19,20] supplied with the code were used to represent the ion core of the atoms. The pseudopotentials for the metal atoms (M=Mo, W, Cr, Ti, and V) where the semicore *p* states are treated as valence was used. Well-converged cutoff energies of 400 eV were used to expand the plane wave basis. The Perdew-Burke-Ernzerhof functional[21,22] was adopted for generalized gradient approximation. Self-consistent structure relaxations were performed with respect to total energy by conjugate-gradient[23,24] optimization for all atomic coordinates as well as for the supercell volume. The supercell containing the oxometalloporpyrin or oxometalloporphyrin dioxygen was constructed as $20\times20\times20$ Å^3 unit cells, so that the molecules are not influenced by the molecules in the neighboring unit cells. In order to estimate the total energy of the isolated system in a vacuum from the small supercell calculations, we made all direction dipole and quadrupole corrections in the total energy.[25]

III. RESULTS AND DISCUSSION

A. Structures of oxometalloporphyrins

We start our discussion by analyzing the structures of oxometalloporphyrins, as shown in Fig. 1(a). M refers to the metal atom in the center of the porphyrin ring; N1, N2, N3, and N4 are the nitrogen atoms, and O1, O2, and O3 are the oxygen atoms. The white spheres are the carbon atoms, and the other small spheres are the hydrogen atoms. Full geometry optimizations are performed for MoO(por), WO(por), TiO(por), VO(por), and CrO(por). The structural parameters after full geometry optimization of these oxometalloporphyrins are shown in Table I. The bond lengths are in angstroms and angles in degrees. The "Calc." column gives the calculated structural parameters and the "Expt." column gives the experimental structural parameters determined by x-ray diffraction (XRD).[24–27] The symbols M, O1, N1, N2, N3, and N4 are of the same meaning as Fig. 1. M-N_p shows the average of the distances between M and the planes formed by all three-atom combinations of the four nitrogen atoms, N1, N2, N3, and N4. Experimental structural parameters in MoO(por), TiO(por), VO(por), and CrO(por) are from MoO(ttp),[11,26] TiO(oep),[11,27] VO(oep),[11,28] and CrO(tpp).[11,29] It is found that the structural parameters of all oxometalloporphyrins are in good agreement with the experimental results by XRDs. Both the calculation results and the experimental results of TiO(por), VO(por), and CrO(por) show that the bond lengths of M–O1, M–N1(2–4), and M–N_p decrease as we proceed to the right of the Periodic Table. This trend is due to differences in atomic radii, which are 1.47 Å for Ti, 1.32 Å for V, and 1.25 Å for Cr. For Cr, Mo, and W, the M–O1 bond length, M–N1(2–4) bond length in CrO(por) are shorter than those in MoO(por) and WO(por), and there is not a large difference between those of MoO(por) and WO(por). This trend can also be explained by similarities in atomic radii, which are 1.36 Å for Mo and 1.37 Å for W.

B. Stabilities of oxometalloporphyrin dioxygen compounds

As a second step in our study, we analyze oxometalloporphyrin dioxygen compounds to examine their stability. Full geometry optimizations of side-on [Fig. 1(b)] and end-on configurations [Fig. 1(c)] were performed in each case. The symbols M, O1, N1, N2, N3, and N4 are the same as in Fig. 1(a), and O2 and O3 are the oxygen atoms originally from the coming O_2 molecule. Table II shows the binding energies. " ****" means that we could not find the stable or metastable state in the corresponding configurations. The

TABLE I. Structure parameters of MoO(por), WO(por), TiO(por), VO(por), and CrO(por). The bond lengths are in Å and angles in degrees. "Calc." abbreviates the calculation structure parameter in this work and "Expt." does the experimental structure parameter by XRD (Refs. 26–29). The symbols M, O1, N1, N2, N3, and N4 are the same meaning as Fig. 1(a). M–N_p shows the average of the distance between M and the planes formed by all three atom combinations of the four nitrogen atoms, N1, N2, N3, and N4.

	MoO(por)		WO(por)		TiO(por)		VO(por)		CrO(por)	
Complex	Calc.	Expt.[a]	Calc.	Expt.	Calc.	Expt.[b]	Calc.	Expt.[c]	Calc.	Expt.[d]
M–O1	1.69	1.656(6)	1.71		1.64	1.613(5)	1.61	1.620(2)	1.57	1.572(6)
M–N1	2.14	2.113(9)	2.12		2.13	2.112(5)	2.10	2.097(3)	2.06	2.028(8)
M–N2	2.14	2.110(11)	2.12		2.13	2.116(5)	2.10	2.102(3)	2.06	2.031(7)
M–N3	2.14	2.104(9)	2.12		2.13	2.120(5)	2.10	2.099(3)	2.06	2.032(7)
M–N4	2.14	2.115(110)	2.12		2.13	2.109(4)	2.10	2.110(3)	2.06	2.037(8)
M–N	0.635	0.6389(8)	0.606		0.592	0.555(6)	0.556	0.543	0.504	0.469
∠O1–M–N1	107	105.54(41)	106		106	104.5(2)	105		104	104.5(4)
∠O1–M–N2	107	109.57(41)	106		106	106.3(2)	105		104	100.6(4)
∠O1–M–N3	107	107.73(42)	106		106	105.8(2)	105		104	105.7(4)
∠O1–M–N4	107	107.55(40)	106		106	104.2(2)	105		104	102.5(4)

[a]Reference 26.
[b]Reference 27.
[c]Reference 28.
[d]Reference 29.

calculation results indicate that the binding energies of MoO(por)(O_2) and WO(por)(O_2) are positive and both complexes take a more stable side-on dioxygen configuration. We think that the reaction of MoO(por) or WO(por) with O_2 can occur: On the other hand, the binding energies of TiO(por) ×(O_2), VO(por)(O_2), and CrO(por)(O_2) are negative, and so one may think that the reaction of TiO(por), VO(por), or CrO(por) with O_2 can hardly occur. The calculation results show that both MoO(por)(O_2) and WO(por)(O_2) take the side-on dioxygen configuration. This is in agreement with experimental results.[12,30] As compared to the binding energy of the Mo complex, it is found that the W complex is more stable.

C. Reactivity of MoO(por) and WO(por) with a side-on O_2

The calculated potential energy profile for the reaction of MoO(por) with a side-on O_2 as a function of the distance between the Mo atom and the coming O_2 center of mass (O_2 c.m.) is presented in Fig. 2. Energies are given in eV relative to the total energies of separate O_2 and MoO(por) molecules. The optimized structures and the O–O distances of the coming O_2 at the characteristic distances of Mo–O_2 c.m. are shown in the balloons in Fig. 2. First the O_2 reaches to the metastable point A, with the O–O distance of 1.25 Å as compared with the gaseous O–O distance of 1.21 Å. As the O1 atom begins to lean to the N1 side at point A, the potential energy begins to increase toward an activation barrier. Then O_2 encounters an activation barrier of about 0.259 eV at point B, with the O–O distance of 1.31 Å. We think that an activation barrier is due to the electron repulsion between the O1 atom and the coming O_2 molecule but is much small due to energy stabilization caused by the Mo–O2 bond and Mo–O3 bond. Finally, the reaction of MoO(por) with a side-on O_2 ends up at point C, with the O–O distance of 1.42 Å. It is found that the O–O distance increases as O_2 approached the Mo atom. The Mo–O1 bond length hardly changes before and after the reaction.

The calculated potential energy profile for the reaction of WO(por) with a side-on O_2 as a function of the distance

TABLE II. Calculation results of the binding energies of oxometalloporphyrin dioxygens. "side-on" in dioxygen configuration gives the configuration like Fig. 1(b) and "end-on" does the configuration like Fig. 1(c). "****" shows that the oxometalloporphyrin and O_2 result separated after the full geometry optimization.

Reaction	Dioxygen configuration	Binding energy [eV]	Stability
MoO(por)+O_2→MoO(por)(O_2)	Side-on	0.611	Stable
	End-on	−0.153	metastable
WO(por)+O_2→WO(por)(O_2)	Side-on	1.400	Stable
	End-on	0.322	Metastable
TiO(por)+O_2→TiO(por)(O_2)	Side-on	−1.156	Metastable
	End-on	****	Unstable
VO(por)+O_2→VO(por)(O_2)	Side-on	−0.517	Metastable
	End-on	****	Unstable
CrO(por)+O_2→CrO(por)(O_2)	Side-on	−0.993	Metastable
	End-on	−1.129	Metastable

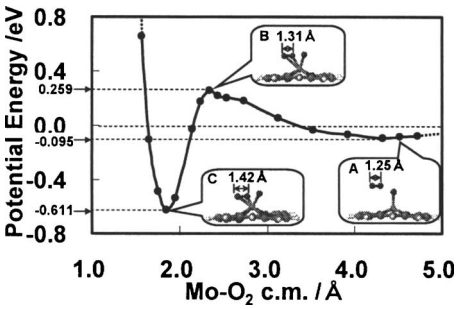

FIG. 2. Calculated potential energy profile for the reaction of MoO(por) with a side-on O_2 as a function of the distance between the Mo atom and the O_2 c.m. Energies are given in eV relative to the value at the point where O_2 is sufficiently far and does not interact with MoO(por). The optimized structures and the O–O distances of the coming O_2 at the characteristic distances of Mo–O_2 c.m. are shown in the balloons.

between the W atom and the O_2 c.m. is presented in Fig. 3. Energies are given in eV relative to the total energies of separate O_2 and WO(por) molecules. The optimized structures and the O–O distances of the coming O_2 at the characteristic distances of W–O_2 c.m. are shown in the balloons in Fig. 3. First the O_2 reaches to the metastable point D, with the O–O distance of 1.25 Å as compared with the gaseous O–O distance of 1.21 Å. As the O1 atom begins to lean to the N1 side at point D, the potential energy begins to increase toward an activation barrier. Then O_2 encounters an activation barrier of about 0.184 eV at point E, with the O–O distance of 1.30 Å. We think that the reaction of WO(por) with a side-on O_2 occurs more easily than that of MoO(por) with a side-on O_2 since this activation barrier is smaller than that of MoO(por). We also think that the reason for this activation barrier is of the same case as MoO(por). Finally, the reaction of WO(por) with a side-on O_2 ends up at point F, with the O–O distance of 1.45 Å. As in the case of the reaction of MoO(por) with a side-on O_2, the O–O distance increases as O_2 approached the W atom.

In the following, we compare activation barriers of the reversible reactions liberating O_2, for MoO(por) and WO(por) with a side-on O_2. The activation barrier of the reversible reaction for MoO(por) with a side-on O_2 is 0.870 eV in Fig. 2, whereas that for WO(por) with a side-on O_2 is 1.584 eV in Fig. 3. The difference in these activation barriers is consistent with the experimental results that photoirradiation with visible light or heating of Mo ^{VI}O(tmp)$\times$(O_2) regenerates Mo ^{VI}O(tmp) by liberating O_2, while

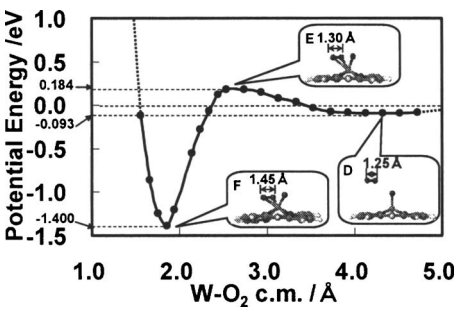

FIG. 3. Same as Fig. 2 but for WO(por) with a side-on O_2.

TABLE III. Same as Table I but for MoO(por)(O_2) and WO(por)(O_2). The symbols M, O1, O2, O3, N1, N2, N4, and M–N_p are the same as in Figs. 1(b) and 1(c).

	MoO(por)(O_2)		WO(por)(O_2)	
Complex	Calc.	Expt.[a]	Calc.	Expt.[b]
M–O1	1.71	1.697(13)	1.73	1.752(13)
M–O2	1.98	1.945(18)	1.96	1.909(15)
M–O3	1.98	1.948(19)	1.96	1.909(15)
M–N1	2.27	2.256(7)	2.28	2.287
M–N2	2.17	2.116(7)	2.16	2.092
M–N3	2.43	2.320(6)	2.44	2.298
M–N4	2.17	2.12(7)	2.16	2.086
O2–O3	1.42	1.42(3)	1.45	1.36(1)
M–N	1.04	1.00	1.05	1.49
∠O1–M–N1	78		77	
∠O2–M–N3	73		73	
∠O3–M–N3	73		73	

[a]Reference 12.
[b]Reference 30.

W ^{VI}O(tmp)(O_2) does not.[10] We think that the reverse reaction would not occur as the activation barrier of the W complex is too large.

D. Structures of MoO(por)(O_2) and WO(por)(O_2)

Table III shows the structural parameters of MoO(por)$\times$(O_2) and WO(por)(O_2). For MoO(por)(O_2), the two bonds, Mo–N1 and Mo–N3, are eclipsed by the oxoligand and the O_2 ligand of the coming O_2, and these bond lengths are slightly longer than those of the other two bonds, Mo–N2 and Mo–N4. The bond lengths of Mo–O2 and that of Mo–O3 are completely equal, and both are longer than that of Mo–O1. The bond length of O2–O3 is 1.42 Å, and longer than that of gaseous O_2. We think that long O2–O3 bond length makes the O2–O3 bond weak and next reaction for water-forming reaction easier. Compared to MoO(por), the Mo atom moves about 0.40 Å out of the N plane because of the attraction by O_2. These bond lengths and the configuration are almost equal to those obtained by XRD (Ref. 12) though the complex used in experiment has four mesityl groups.

For WO(por)(O_2), W–N1 and W–N3 are likewise eclipsed by the oxoligand and the O_2 ligand of the coming O_2, and these bond lengths are slightly longer than W–N2 and W–N4. The bond length of W–O2 and that of W–O3 are completely equal, and both are longer than that of W–O1. The bond length of O2–O3 is 1.45 Å, and longer than that of gaseous O_2. We think that long O2–O3 bond length makes the O2–O3 bond weak and next reaction for water-forming reaction easier. Compared to WO(por), the W atom moves about 0.44 Å out of the N plane because of the attraction by O_2. The bond lengths of W–O1 and W–N1 are almost in agreement with those of XRD,[30] but there are differences between calculated and XRD results for the other bond lengths. Particularly, the W–N_p distance obtained by XRD is about 1.4 times larger than our calculated result. Our calculated results show that each structural parameter in WO(por)(O_2) is similar to that in MoO(por)(O_2) in the same

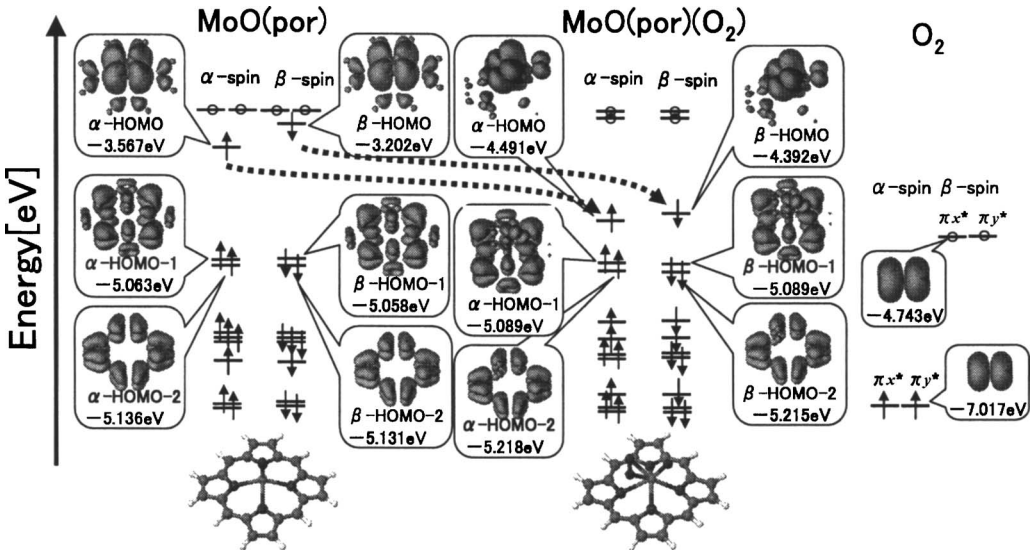

FIG. 4. Molecular orbital energy diagrams and schematic valence electron densities for MoO(por), MoO(por)(O_2), and O_2 in the order from left hand side to right hand side. The energy is measured from vacuum level. For each molecule, the left hand side of the molecular orbital energy diagram shows molecular orbitals for α-spin electrons, and the right hand side shows molecular orbitals for β-spin electrons. The schematic electron densities of $\alpha(\beta)$-HOMO, $\alpha(\beta)$-HOMO-1, and $\alpha(\beta)$-HOMO-2 of MoO(por) and MoO(por)(O_2) are drawn with a contour surface cutoff at 0.003 $e/\text{Å}^3$.

manner that each structure parameter WO(por) is similar as that in MoO(por). The similarity between the atomic radii of W (1.37 Å) and Mo (1.36 Å) may support our calculated geometry.

E. Molecular orbitals of MoO(por), WO(por), and their dioxygen compounds

Figure 4 gives molecular orbital energy diagrams and schematic valence electron densities for MoO(por), MoO(por)(O_2), and O_2 in the order from left to right. The energy is measured from vacuum level. For each molecule, the left hand side of the molecular orbital energy diagram shows molecular orbitals for α-spin electrons, and the right hand side shows molecular orbitals for β-spin electrons. The schematic electron densities of $\alpha(\beta)$-HOMO (highest occupied molecular orbital), $\alpha(\beta)$-HOMO-1, and $\alpha(\beta)$-HOMO-2 of MoO(por) and MoO(por)(O_2) are drawn with contour surfaces cutoff at 0.003 $e/\text{Å}^3$. By analyzing the results of electron densities, it is found that the $\alpha(\beta)$-HOMO of MoO(por) are mainly made of the d orbitals of Mo atom and those of MoO(por)(O_2) are mainly the π^* orbitals of the adsorbed O_2 which are also called the antibonding molecular orbitals. There two observations suggest that electron charge is transferred from MoO(por) to O_2, thereby populating the antibonding states of O_2 and weakening the O–O bond. As a result, the O–O bond becomes longer after O_2 molecule adsorbs. The transfer of the electrons from the d orbitals of the Mo atom to O1 [the original oxygen of MoO(por)] is hardly seen. The electron densities of $\alpha(\beta)$-HOMO-1 in MoO(por) and MoO(por) (O_2) are almost the same. Likewise, the electron densities of $\alpha(\beta)$-HOMO-2 in MoO(por) and MoO(por) (O_2) are almost the same. Very few dioxygen character are seen in the $\alpha(\beta)$-HOMO-1 and $\alpha(\beta)$-HOMO-2 of MoO(por) (O_2); most of the electrons stay around the porphyrin ring of the original MoO(por). Therefore, our results support that electrons transfer from the d orbitals of the Mo atom to the π^* orbitals of the coming O_2 during the adsorption of O_2 on MoO(por).

Next, the difference in energy between the α-HOMO and β-HOMO of MoO(por) is about 0.365 eV, whereas that in MoO(por) (O_2) is about 0.099 eV. It is also found that the α-HOMO becomes more stable by about 0.924 eV after adsorption of O_2 and the β-HOMO stabilizes by about 1.190 eV.

Figure 5 gives the molecular orbital energy diagrams and the schematic electron densities for WO(por), WO(por)(O_2), and O_2 in the order from left to right. The symbols, labels, and conditions are the same as in Fig. 4. The schematic electron densities of the W complexes are almost the same as those of the Mo complexes. Therefore, as is the case of Mo complexes, it is found that the electrons transfer from the HOMOs of the W complex (d orbitals of the W atom) to the π^* orbitals of the coming O_2 during the adsorption of O_2 to WO(por).

Next, there is no significant difference of the energy between the α-HOMO and β-HOMO in WO(por), whereas the difference of the energy between the α-HOMO and β-HOMO in WO(por) (O_2) is about 0.096 eV. It is found that the α-HOMO becomes more stable by about 1.322 eV after the adsorption of O_2 on WO(por), and β-HOMO stabilizes by about 1.227 eV.

Comparison of the energy difference between the HOMOs of Mo complexes with that of W complexes indicates that MoO(por) cannot become more stable than WO(por) by adsorption of O_2 since it has naturally more stable α-HOMO than WO(por).

IV. CONCLUSION

We have investigated oxometalloporpyhrins [MoO(por), WO(por), TiO(por), VO(por), and CrO(por)] and the stability of O_2 adsorption on these complexes by using density-

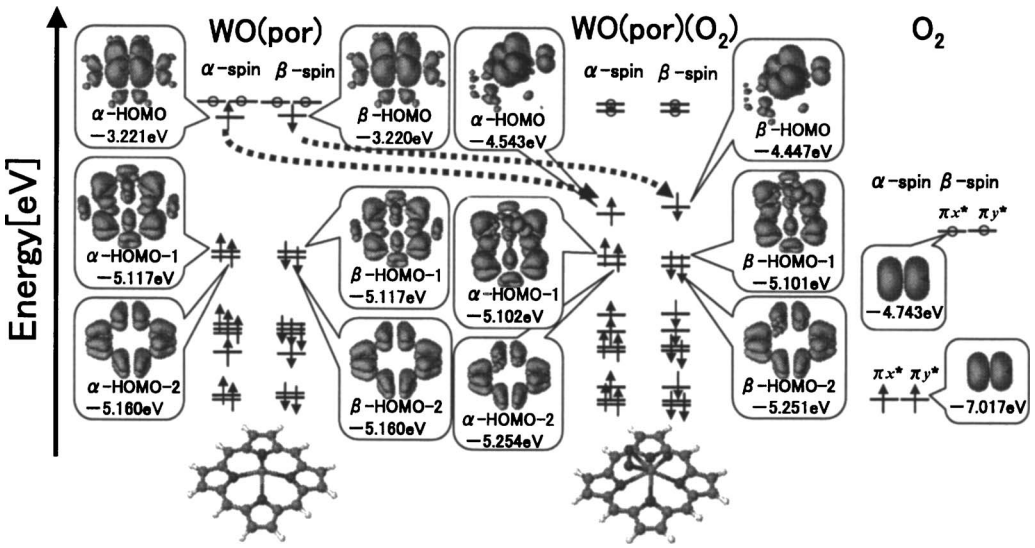

FIG. 5. Same as Fig. 4 but for WO(por), WO(por)(O_2), and O_2.

functional theory calculations. The structural parameters of the above complexes are in agreement with the experimental results by XRD. Our calculations showed that MoO(por) and WO(por) can undergo reactions with O_2, but TiO(por), VO(por), and CrO(por) cannot. It was found that the coordinated O_2 for MoO(por) and WO(por) takes a side-on configuration than an end on. The O–O bond lengths of the O_2 adsorbed on these complexes are more than 1.4 Å.

Next, we calculated the potential energy profiles of MoO(por) and WO(por) that the O_2 addition reaction would occur. Activation barriers for the reactions of MoO(por) and WO(por) with a side-on O_2 are much smaller than their reverse reactions. The activation barrier for the reaction of WO(por) with a side-on O_2 is smaller than that of MoO(por) and hence WO(por) has greater reactivity with O_2 than MoO(por). We think that activation barriers of the O_2 addition reactions of MoO(por) and WO(por) are due to the electron repulsion between the original O atom and the coming O_2 molecule. The activation barrier for the reverse reaction of WO(por)(O_2) liberating O_2 is about twice that for MoO(por)(O_2). This indicates that the Mo–O bonds [two bonds between the Mo atom and O atoms of the coming O_2 molecule] of MoO(por) are much weaker than the case of W–O. The experimental results that photoirradiation with visible light or heating of Mo ^{VI}O(tmp)(O_2) regenerates Mo ^{VI}O(tmp) by liberating O_2 while W ^{VI}O(tmp)(O_2) does not[10] are explained by the difference in activation barriers of the reverse reactions. We think that MoO(por) and WO(por) have a potential for water-forming reaction since their O_2 adducts have the O–O bond lengths longer than gaseous O_2. In addition, we assume that the reaction activity of water-forming reaction of MoO(por) would be higher than the case of WO(por) since the activation barrier of the reversible reaction liberating O_2 of MoO(por)(O_2) is much smaller than the case of WO(por)(O_2). From these reasons, we think that MoO(por) is more appropriate than WO(por) as the cathode electrode of the PEFC.

From the viewpoint of molecular orbitals, it was found that the orbitals that contribute to the O_2 addition reactions of MoO(por) and WO(por) are mainly HOMOs. The HOMOs of the MoO(por) and WO(por) were the same and were made of the *d* orbitals of the metal atom. On the other hand, the HOMOs of the MoO(por)(O_2) and WO(por)(O_2) were the same and were made of the π^* orbitals of the coming O_2. Therefore, this resulted in a transfer in electrons from the *d* orbitals of the metal atom to the π^* orbitals of the coming O_2 in the O_2 addition reactions for MoO and WO(por).

ACKNOWLEDGMENTS

This work is supported by the Ministry of Education, Culture, Sports, Science and Technology of Japan (MEXT) through their Grant-in-Aid for Scientific Research on Priority Areas (Developing Next Generation Quantum Simulators and Quantum-Based Design Techniques) and Special Coordination Funds for the 21st Century Center of Excellence (COE) Program (G18) "Core Research and Advance Education Center for Materials Science and Nano-Engineering." One of the authors (E.D.) wishes to thank The Rotary Yoneyama Memorial Foundation, Inc. for his scholarship. Some of the calculations were done using the computer facilities of the Cybermedia Center (Osaka University), the ISSP Super Computer Center (University of Tokyo), the Yukawa Institute (Kyoto University), and the Japan Atomic Energy Research Institute (ITBL, JAERI).

[1] M. Tsuda, E. S. Dy, and H. Kasai, J. Chem. Phys. **122**, 244719 (2005).
[2] E. S. Dy and H. Kasai, Chem. Phys. Lett. **422**, 539 (2006).
[3] M. Tsuda, W. A. Diño, and H. Kasai, Solid State Commun. **133**, 589 (2005).
[4] M. Tsuda, E. S. Dy, and H. Kasai, Eur. Phys. J. D **38**, 139 (2006).
[5] B. Steiger and F. C. Anson, Inorg. Chem. **33**, 5767 (1994).
[6] M. Yuasa, B. Steiger, and F. C. Anson, J. Porphyr. Phthalocyanines **1**, 180 (1997).
[7] C. J. Chang, Z.-H. Loh, C. Shi, F. C. Anson, and D. G. Nocera, J. Am. Chem. Soc. **126**, 10013 (2004).
[8] S. Fukuzumi, K. Okamoto, C. P. Gros, and R. Guilard, J. Am. Chem. Soc. **126**, 10441 (2004).
[9] M. Inaba, 14th International Conference on the Properties of Water and Steam in Kyoto, 2006 (unpublished).
[10] J. Tachibana, T. Imamura, and Y. Sasaki, Bull. Chem. Soc. Jpn. **71**, 363

(1998).
[11] Abbreviations: ttp=5, 10, 15, 20-tetra-p-tolylporphyrinato, oep=2, 3, 7, 8, 12, 13, 17, 18-octaethylporphrinato, tpp=5, 10, 15, 20-tetraphenylporphyrinato, tmp=5, 10, 15, 20-tetramesitylporphyrinato.
[12] T. Fujiwara, N. H. Rees, K. Umakoshi, J. Tachibana, Y. Sasaki, W. McFarlane, and T. Imamura, Chem. Lett. **2000**, 102.
[13] J. P. Collman, R. R. Gagne, C. A. Reed, W. T. Robinson, and G. A. Rodley, Proc. Natl. Acad. Sci. U.S.A. **71**, 1326 (1974).
[14] C. Rovira, P. Ballone, and M. Parrinello, Chem. Phys. Lett. **271**, 247 (1997).
[15] G. Kresse and J. Hafner, Phys. Rev. B **47**, 558 (1993).
[16] G. Kresse and J. Hafner, Phys. Rev. B **49**, 14251 (1994).
[17] G. Kresse and J. Furthmüller, Comput. Mater. Sci. **6**, 15 (1996).
[18] G. Kresse and J. Furthmüller, Phys. Rev. B **54**, 11169 (1996).
[19] D. Vanderbilt, Phys. Rev. B **41**, 7892 (1990).
[20] G. Kresse and J. Hafner, J. Phys.: Condens. Matter **6**, 8245 (1994).
[21] J. P. Perdew, K. Burke, and M. Ernzerhof, Phys. Rev. Lett. **77**, 3865 (1996).
[22] J. P. Perdew, K. Burke, and M. Ernzerhof, Phys. Rev. Lett. **78**, 1396 (1997).
[23] M. P. Teter, M. C. Payne, and D. C. Allan, Phys. Rev. B **40**, 12255 (1989).
[24] D. M. Bylander, L. Kleinman, and S. Lee, Phys. Rev. B **42**, 1394 (1990).
[25] G. Makov and M. C. Payne, Phys. Rev. B **51**, 4014 (1995).
[26] T. Diebold, B. Chevrier, and R. Weiss, Inorg. Chem. **18**, 1193 (1979).
[27] R. Guilard, J. M. Latour, C. Lecomte, J. C. Marchon, J. Protas, and D. Ripoll, Inorg. Chem. **17**, 1228 (1978).
[28] F. S. Molinaro and J. A. Ibers, Inorg. Chem. **15**, 2278 (1976).
[29] T. Groves, W. J. Kruper, Jr., R. C. Haushalter, and W. M. Butler, Inorg. Chem. **21**, 1363 (1982).
[30] C. Yang, S. J. Dzugan, and V. L. Goedken, J. Chem. Soc., Chem. Commun. **1985**, 1425.